

LETTERS

Design principles of a bacterial signalling network

Markus Kollmann¹, Linda Løvdok², Kilian Bartholomé¹, Jens Timmer^{1,3} & Victor Sourjik²

Cellular biochemical networks have to function in a noisy environment using imperfect components. In particular, networks involved in gene regulation or signal transduction allow only for small output tolerances, and the underlying network structures can be expected to have undergone evolution for inherent robustness against perturbations¹. Here we combine theoretical and experimental analyses to investigate an optimal design for the signalling network of bacterial chemotaxis, one of the most thoroughly studied signalling networks in biology. We experimentally determine the extent of intercellular variations in the expression levels of chemotaxis proteins and use computer simulations to quantify the robustness of several hypothetical chemotaxis pathway topologies to such gene expression noise. We demonstrate that among these topologies the experimentally established chemotaxis network of *Escherichia coli* has the smallest sufficiently robust network structure, allowing accurate chemotactic response for almost all individuals within a population. Our results suggest that this pathway has evolved to show an optimal chemotactic performance while minimizing the cost of resources associated with high levels of protein expression. Moreover, the underlying topological design principles compensating for intercellular variations seem to be highly conserved among bacterial chemosensory systems².

Errors in signal transduction can lead to wrong development and behavioural decisions, and result in growth impairment or, in multicellular organisms, cancer¹. Therefore one expects a strong selective pressure towards networks showing intrinsic robustness against the various sources of inter- and intracellular perturbations, such as fluctuations in protein concentration. Owing to limitations in our quantitative understanding of most signalling networks, only few detailed studies of network robustness are currently available^{3–6}. In the simple signalling system of bacterial chemotaxis, activity of receptors on the cell surface is regulated by changes in ambient ligand concentration^{7,8}. Active receptors enhance autophosphorylation activity of the receptor-associated kinase CheA, which transmits the signal to the flagellar motors by phosphorylating a diffusible response regulator protein CheY. One of the key features of the chemotaxis pathway is precise adaptation—its ability to return to the same level of pathway activity under conditions of continuous stimulation. Failure of this systems property can lead to permanent swimming or tumbling behaviour and thus would restrict chemotactic response to a narrow range of chemoeffector concentrations. The most simple topology of a chemotactic signalling network that allows for precise adaptation is a two-state model proposed in ref. 3 (BL model). This model is schematically drawn in Fig. 1a. The core property of the model is that receptors can be reversibly methylated. A higher level of methylation increases the probability of a receptor to switch to an active state and thus balances the inhibiting effect of attractants. Almost perfect adaptation results from a constantly working methyltransferase (CheR) balanced by a methylesterase (CheB), which works only on active receptors⁹.

The BL model can readily explain the robustness of precise adaptation against a wide range of variations in kinetic parameters and protein concentrations as a consequence of integral feedback control at the methylation level^{3,9}. However, precise adaptation would be only physiologically relevant when the adapted level of CheY-P falls within the working range of the flagellar motor¹⁰. It is thus the stationary level of CheY-P rather than precise adaptation per se that should be under evolutionary selection, but in the BL model this quantity is not robust to large perturbations⁴.

By extending the BL model, it is possible to construct larger adaptive topologies having equal input–output characteristics (Fig. 1b–d) and analyse their robustness against intercellular variations in protein concentrations arising from protein synthesis. The latter represents the dominating source of variations in a bacterial cell population^{11,30}. Such intercellular variations can persist on the generation timescale because there is no evidence for an active degradation of chemotaxis proteins under standard growth and assay conditions, and the decrease in protein levels mainly results from dilution during cell division¹².

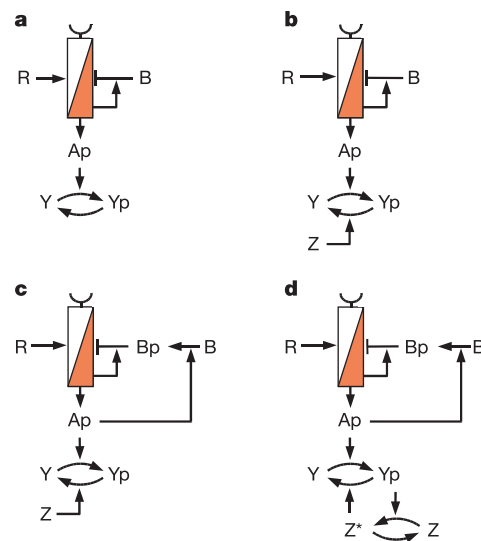


Figure 1 | Four possible network topologies of bacterial chemotaxis showing precise adaptation. Links between proteins indicate activations (arrows) or repressions (bar ends). The receptor can either be in an active state (red) or an inactive state (white). The proteins involved are denoted, for example, by A = CheA, and their phosphorylated forms by Ap = CheA-P. **a**, Minimal model as proposed in ref. 3. **b**, Same as model **a** but with a phosphatase CheZ substituting auto-phosphorylation of CheY-P in topology **a**. **c**, Same as model **b** but only the phosphorylated form of CheB can form a complex with active receptors. This topology represents the experimentally established network of *E. coli*. **d**, Same as topology **c** but with an active form (Z^*) of the CheY phosphatase^{27,28}.

¹Institut für Physik, Universität Freiburg, Hermann-Herder-Str. 3, D-79104 Freiburg, Germany. ²ZMBH, University of Heidelberg, Im Neuenheimer Feld 282, D-69120 Heidelberg, Germany. ³FDM, Universität Freiburg, Eckerstr. 1, D-79104 Freiburg, Germany.

To measure experimentally the amplitude of such intercellular variations in the levels of chemotaxis proteins, we replaced a native *cheY* gene in *E. coli* with *cheY* fused to a yellow fluorescent protein (*cheY-eyfp*) as a translational reporter. The reporter construct is thus expressed from the native promoter as part of polycistronic messenger RNA of the *meche* operon that also encodes Tar and Tap chemoreceptors, and most cytosolic chemotaxis proteins (Supplementary Fig. S1). CheA and CheW are expressed as part of another (*mocha*) operon. The protein levels in the population (Fig. 2a) show large intercellular variation with an apparently asymmetric distribution, consistent with previous observations¹². The gene expression noise $\eta = \sigma/n$, where σ is the standard deviation and n is the mean expression, depends on the level of gene transcription, and decreases from 0.67 to 0.47 upon deletion of the upstream transcription inhibitor, the anti-sigma factor FlgM^{13,14} (Fig. 2a). Recently, model-based analysis showed that transcription should dominate gene expression noise between proteins when expressed from the same mRNA transcript^{15,16}. We confirmed this conclusion by comparing the variation in the levels of CheY and CheZ expressed as fusions to yellow and cyan fluorescent proteins (YFP and CFP) from the same promoter in the same order as they are positioned on the chromosome and under their native ribosome-binding sequences (Fig. 2b). There is a strong co-variation in the expression levels of both, which arises from fluctuations in transcriptional activity, and only a moderate independent variation as a consequence of stochastic effects in both transcription and translation^{11,17}. Proteins expressed from two different chemotaxis operons, *mocha* and *meche*, which belong to the same regulon, also show significant co-variation

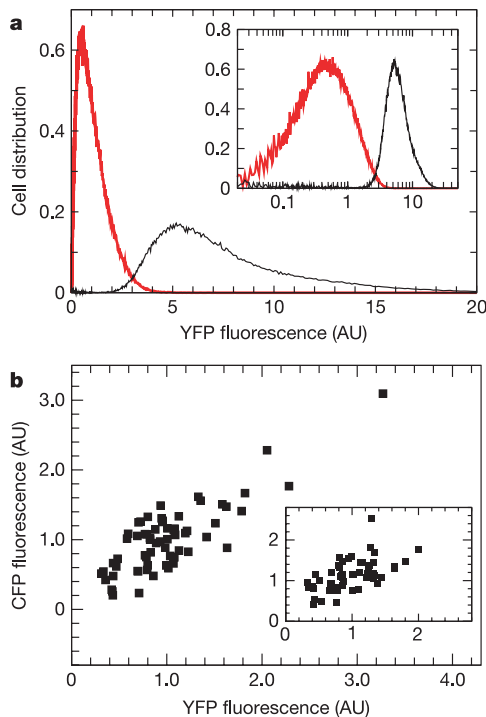


Figure 2 | Gene expression noise of the chemotaxis proteins. Intercellular variations in the level of CheY, expressed as a YFP fusion from the native chromosomal position. The distribution of wild-type (black line) and *flgM* (red line) cells is characterized by the means 1 and 6.6 and standard deviations 0.67 and 3.17, respectively. Inset: same data normalized to the same maximum intensity and displayed on a logarithmic scale. **b**, Correlation of the expression of CheY–YFP and CheZ–CFP from a single pTrc promoter without induction. Values for uncorrelated and concerted variations of the gene expression noise are $\eta_{in} = 0.20$ and $\eta_{ex} = 0.44$, respectively. Inset: correlation of the expression of CheY–YFP and CheA–CFP from the native chromosomal positions, with $\eta_{in} = 0.26$ and $\eta_{ex} = 0.35$. AU, arbitrary units.

in gene expression noise (Fig. 2b inset) but with a 25% increase of independent variations in comparison with proteins expressed from the same operon.

We further experimentally determined the effect of co-variation in the levels of all signalling proteins on chemotactic behaviour (Fig. 3). Concerted overexpression of all proteins up to 6.6-fold above the native level had little effect on chemotaxis efficiency, as measured by a chemotaxis-driven spreading of bacteria in an attractant gradient created by nutrient depletion in soft agar (swarm assay). Thus, the CheY-P concentration in the overexpressing cells must be in the working range of the flagellar motor. This conclusion was further confirmed by the observation that the average time the motor spends rotating clockwise (clockwise bias) was nearly unaffected by protein overexpression (Fig. 3b). Notably, the corresponding standard deviation decreased with the level of expression, as expected from the decline in strength of gene expression noise (Fig. 2 and Supplementary Fig. S3).

Relying on these experimental data, we analysed mathematically the robustness of the four network topologies drawn in Fig. 1 under conditions of physiological perturbations. Owing to a steep response of the flagellar motor¹⁰, the level of CheY-P in adapted cells can vary only about one-third from its optimal value. Outside this concentration regime the cell mainly tumbles or swims continuously and cannot properly respond to stimuli. For example, a fully tumbling cell cannot respond to repellents and has a reduced sensitivity to attractants. The chemotactic efficiency of a population therefore depends on the fraction of bacteria for which the CheY-P levels are within these limits. We tested the different hypothetical network topologies, shown in Fig. 1, for their ability to reproduce qualitatively the experimental data for concerted variations of mean expression levels (Fig. 3). In the computer simulations, we used the experimentally determined gene expression noise (Fig. 2) as an estimate for the minimum intercellular variations. The established topology for *E. coli* (Fig. 1c) reproduces accurately the experimental data, whereas the simpler topology (Fig. 1a) fails to match the data. To quantify further the robustness of the different network topologies, we calculated the fraction of fully chemotactic bacteria for different strengths of gene expression noise (Fig. 4). The topologies in Fig. 1c, d allow for

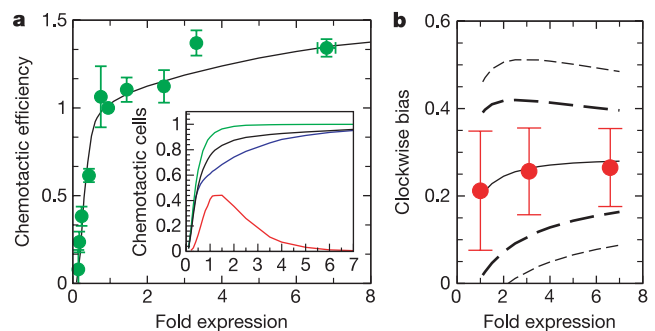


Figure 3 | Effect of the total concentration of signalling proteins on chemotaxis. **a**, Chemotaxis efficiency of *flgM* (VS102) cells, expressing varying levels of FlgM from a plasmid, determined in a swarm assay and normalized to the value of wild-type (RP437) cells. The relative mean expression of chemotaxis proteins at each FlgM level was measured as in Fig. 2a, using the LL1 strain as a reporter. The solid line is a guide to the eye, and error bars indicate standard errors. Inset: simulated fraction of fully chemotactic cells for topologies in Fig. 1a (red line), b (blue line), c (black line) and d (green line). **b**, Clockwise motor bias as a function of expression of chemotaxis proteins. Each point represents a mean of 20–30 cells. Error bars indicate standard deviations and illustrate intercellular variation. The solid line shows the clockwise bias calculated from the mathematical model of Fig. 1c under gene expression noise estimated from Fig. 2. The calculated standard deviation is depicted for the topology in Fig. 1c, assuming a steepness of the motor response curve with a Hill coefficient of five²⁹ (thick dashed lines) or ten¹⁰ (thin dashed lines).

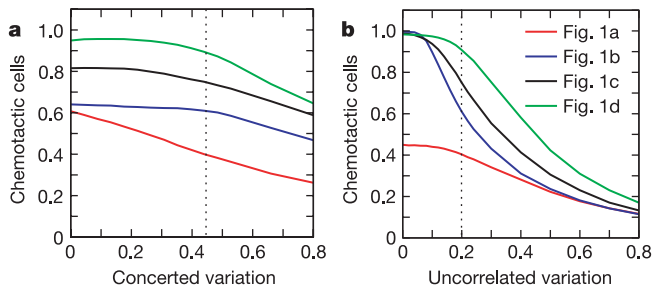


Figure 4 | Simulated fraction of chemotactic cells as a function of gene expression noise. Topologies are marked as in Fig. 3. The native level of gene expression noise is indicated by dotted lines. **a**, Concerted variations ranging up to twofold of the wild-type strength with uncorrelated variations kept at the wild-type value, $\eta_{in} = 0.2$. **b**, Same as **a** but with varying strength of uncorrelated variations and with concerted variations fixed to the wild-type value, $\eta_{ex} = 0.44$.

the highest fraction of cells in the population to respond accurately to changes in ligand concentration. Furthermore, the topologies in Fig. 1b–d are sufficiently robust to compensate for co-variations in expression levels (Fig. 4a) but tolerate only a moderate increase in independent fluctuations in protein concentrations (Fig. 4b).

There are two key features accounting for the higher robustness of the topologies shown in Fig. 1c, d. First, robustness against concerted variations requires a balance of phosphatase and kinase reactions and similar requirements for the methylation process, as shown by mathematical analysis in Box 1. The condition for a robust adaptive chemotaxis pathway is that CheY-P demands a phosphatase (CheZ) whereas CheB-P must not have one. But this kind of robustness is only valid for concentrations larger than the wild-type level (Fig. 3a). The strong decrease in the number of chemotactic bacteria at lower expression levels (Fig. 3a inset) arises because the total CheY concentration drops below the working range of the flagellar motor. The increase in chemotactic performance of the topologies in Fig. 1b–d with the mean expression level can be explained by an accompanying decline of the gene expression noise¹¹ (Fig. 2a and

Box 1 | Robustness against variations in transcriptional activity

A general deterministic description for the concentrations of the N different phosphorylation and methylation states $\mathbf{y}(t) = \{y_1(t), \dots, y_N(t)\}$ of a signalling pathway are given by the equations

$$\partial_t y_i(t) = F_i(\mathbf{y}(t)|\mathbf{x}^T) \quad (1)$$

(see Supplementary Information for details and definitions). The sum over different states, $(y_i)_k$, of the protein with index k is connected to its total concentration by $\sum_{\{y_i\}_k} y_i(t) = x_k^T$. For the stationary solution, $F_i(\mathbf{y}(t)|\mathbf{x}^T) = 0$, to be invariant against co-varying total protein concentrations, for example due to a λ -fold change in transcriptional activity $\mathbf{x}^T = (x_1^T, \dots, x_M^T) \rightarrow (\lambda x_1^T, \dots, \lambda x_M^T)$ of the M chemotaxis proteins, we have to demand homogeneity of F with respect to \mathbf{x}^T ,

$$F_i(\mathbf{y}(t)|\lambda \mathbf{x}^T) = \lambda^{\mu_i} F_i(\mathbf{y}(t)|\mathbf{x}^T) \quad (2)$$

with $\mu_i > 0$. For the equations corresponding to the topology in Fig. 1a the homogeneity condition can not be satisfied. For the topologies in Fig. 1b–d we have the case $F_i(\mathbf{y}(t)|\lambda \mathbf{x}^T) \approx \lambda F_i(\mathbf{y}(t)|\mathbf{x}^T)$ for $\lambda > 1$ and therefore these topologies are invariant against changes in transcriptional activity of signalling proteins at expression levels higher than the wild type. For example, to keep the level of CheY-P invariant under a λ -fold overexpression, the resulting increase of phosphotransfer to CheY has to be balanced by an increase in dephosphorylation rate. This is achieved by a simultaneous upregulation of the phosphatase CheZ. The conditions of invariance and the consequences of their violation are discussed in the Supplementary Information.

Supplementary Fig. S3). The location of the wild-type concentration as shown in Fig. 3a seems to reflect a selective pressure towards overall low protein concentrations¹⁸.

The second topological feature leading to higher swarming efficiency is CheB phosphorylation resulting in an additional negative feedback loop (Fig. 1c, d). As shown in Box 2, this second feedback loop compensates partially for deviations from the optimal CheY-P level without changing the input–output characteristics. CheB phosphorylation has been previously shown to be non-essential for adaptation^{3,4}, and our analysis suggests that its main function might be in noise reduction. The essential features for the two design principles described above seem to be present among most established pathway topologies of bacterial chemotaxis². In particular, the CheB phosphorylation feedback is almost universal, and although many bacteria lack CheZ, the function of CheY phosphatase is taken over by another protein or by the kinase itself. The even higher robustness of the topology in Fig. 1d arises from the activation of CheZ by CheY-P that follows the same noise compensatory mechanism as the CheB phosphorylation feedback.

Box 2 | Error reduction mechanisms

Errors in the output arising from uncorrelated variations of protein levels and deviations from the optimal rate constants can be partially compensated by additional negative feedback loops²² (Fig. 1). Here, we focus on the gain in robustness due to activation of the methyltransferase (CheB) by phosphotransfer from CheA. We simplify the *E. coli* chemotaxis topology (Fig. 1c) such that any receptor has only one methylation site and the average activity of methylated receptors depends on the ambient chemoeffector concentration. Non-methylated receptors remain inactive. Using Michaelis-Menten kinetics, the steady-state equation for the methylation process reads

$$\partial_t T_M = k_R R - k_B B p \frac{T_A}{K_B + T_A} = 0 \quad (3)$$

with k_R and k_B the associated rate constants and K_B the Michaelis-Menten constant for binding of CheB-P to active receptor complexes³. The concentrations of methylated and active receptors are denoted by T_M and T_A , and the concentrations of the methyltransferase and active methyltransferase by R and Bp , respectively. For the topologies in Fig. 1c, d the methyltransferase, CheB, is active only in the phosphorylated form and thus depends on the concentration of the phosphodonor, $Ap = [\text{CheA-P}]$. We have also assumed that the methyltransferase, CheR, works at saturation. The steady-state equation for Ap is given by

$$k_A T_A (A^T - Ap) - k_Y Ap (Y^T - Yp) = 0 \quad (4)$$

with $Yp = k_Y Ap Y^T / (k_Y Ap + k_Z Z)$ and where $k_Z Z$ is the dephosphorylation rate of CheY-P. The superscript T indicates total protein concentrations. In the above equation we neglected the small contribution of the phosphoacceptor CheB as (ref. 23) $k_Y Y^T \gg k'_B B^T$, with k_Y and k'_B the rates of phosphate transfer from CheA-P to CheY and CheB, respectively. As Ap and R are linked through equations (3) and (4), a small increase in the amount of methyltransferase, $R + \Delta R$, results in a change of phosphorylated receptors given by

$$\Delta Ap = \left[\alpha + \beta \frac{\partial Bp}{\partial Ap} \right]^{-1} \gamma \Delta R \quad (5)$$

To arrive at equation (5) we have performed a linear expansion around fixed values for the remaining protein concentrations. The linear expansion coefficients α and β can be shown to have equal sign (see Supplementary Information). The derivative $\partial Bp / \partial Ap > 0$ manifests the higher robustness against perturbations of the network topologies in Fig. 1c, d. This contribution increases the amount of active methyltransferase (CheB-P) whenever the average activity of the receptors is rising, and thus partially compensates for an increased amount of methyltransferase. This term is absent in the topologies of Fig. 1a, b, as here the methyltransferase is not phosphorylated and thus $\partial Bp / \partial Ap = 0$. Fluctuations in other protein levels are compensated for in an equivalent way.

Reflecting strong selection, the chemotaxis pathway in *E. coli* seems to be optimized for high sensitivity, fast response and perfect adaptation^{7,8,19,20}. As shown in this work, the experimentally established design of the chemotaxis network in *E. coli* represents a minimal topology providing high robustness to physiological perturbations. This network design can compensate for the observed strong co-variations in gene expression but the negative effect of uncorrelated variations on the efficiency of chemotaxis can only be attenuated. Similar correlations in expression have been found recently in eukaryotes for genes under identical control²¹. We can therefore expect that analogous design principles, compensating for intercellular variations, will apply to all signalling networks and gene regulation systems whenever precise regulation of an output signal is demanded.

METHODS

Bacterial strains and plasmids. All strains used in this study were derived from a wild-type chemotaxis strain RP437 using a pAMPts homologous recombination system of allele exchange, described before²⁴. Strain VS162 carries a *cheY–eyfp* fusion construct in place of a *cheY* gene on the chromosome, and strain LL6 carries *cheY–eyfp* and *cheA–ecfp* fusion constructs in place of *cheY* and *cheA* genes on the chromosome. Strains VS102 (*flgM*) and LLI (*cheY–eyfp flgM*) carry in-frame deletions of an anti-sigma factor (FlgM) that negatively controls the expression of all chemotaxis and flagellar (class III) genes. Plasmid pLL6 Amp^r encodes FlgM expressed under control of an isopropyl β -D-thiogalactoside (IPTG)-inducible promoter pTrc. Plasmid pVS88 encodes CheY–YFP and CheZ–CFP fusion proteins transcribed as one polycistronic mRNA from the pTrc promoter²⁵. The level of CheY–YFP expression in the absence of IPTG closely matched the expression from a native promoter (VS162).

Growth conditions. All strains were grown under standard chemotaxis conditions at 34 °C in tryptone broth (TB) as described before^{24,25} in the presence of varying amounts of IPTG. Swarm assays were performed at 34 °C on TB plates supplemented with 0.3% agar (Applichem) and indicated concentrations of IPTG.

Quantification of gene expression. Expression of fluorescent reporter proteins in individual cells was quantified using flow cytometry on a FACScan (BD Biosciences) equipped with a 488-nm argon laser, or fluorescence imaging on an Axiovert 200 fluorescence microscope equipped with an ORCA AG CCD camera (Hamamatsu). FACScan data were analysed using CellQuest Pro 4.0.1 software. Imaging data were analysed using ImageJ software (W. Rasband) to quantify fluorescence of the entire cell. When tested on the same population, both methods gave essentially identical results.

Tethering. Cells were tethered to a glass coverslip as described earlier²⁶. The rotation of tethered cells was recorded for 3 min at 25 °C with a microscope (Zeiss AxioStar plus) equipped with a CCD camera (Panasonic WV-BP330) and a DV Recorder (Panasonic AG-DV1DC). The analysis was performed using IPS image recognition software from the Visometrics Group.

Description of the mathematical model. The dynamical behaviour of the networks was described on the level of ordinary differential equations assuming Michaelis–Menten kinetics. The kinetic constants were taken from *in vivo* and *in vitro* measurements, except for the methylation process and the CheY–CheZ feedback loop shown in Fig. 1d, where constants were determined from optimization of a population of 70 cells with respect to their least deviation from the midpoint of the motor response curve¹⁰ (3.2 μ M) under the experimentally determined gene expression noise. Fully chemotactic cells were defined as cells for which the level of CheY–P was within the interval 2.2–4.3 μ M and for determination of their proportion in Figs 3 and 4 a population size of 10⁴ cells was assumed. A detailed description of the mathematical model is given in the Supplementary Information.

Received 25 May; accepted 12 September 2005.

1. Kitano, H. Biological robustness. *Nature Rev. Genet.* **5**, 826–837 (2004).
2. Szurmant, H. & Ordal, G. W. Diversity in chemotaxis mechanisms among the bacteria and archaea. *Microbiol. Mol. Biol. Rev.* **68**, 301–319 (2004).
3. Barkai, N. & Leibler, S. Robustness in simple biochemical networks. *Nature* **387**, 913–917 (1997).

4. Alon, U., Surette, M. G., Barkai, N. & Leibler, S. Robustness in bacterial chemotaxis. *Nature* **397**, 168–171 (1999).
5. von Dassow, G., Meir, E., Munro, E. M. & Odell, G. M. The segment polarity network is a robust developmental module. *Nature* **406**, 188–191 (2000).
6. Eldar, A. *et al.* Robustness of the BMP morphogen gradient in *Drosophila* embryonic patterning. *Nature* **419**, 304–308 (2002).
7. Sourjik, V. Receptor clustering and signal processing in *E. coli* chemotaxis. *Trends Microbiol.* **12**, 569–576 (2004).
8. Wadhams, G. H. & Armitage, J. P. Making sense of it all: bacterial chemotaxis. *Nature Rev. Mol. Cell Biol.* **5**, 1024–1037 (2004).
9. Mello, B. & Tu, Y. Perfect and near-perfect adaption in a model of bacterial chemotaxis. *Biophys. J.* **84**, 2943–2956 (2003).
10. Cluzel, P., Surette, M. & Leibler, S. An ultrasensitive bacterial motor revealed by monitoring signaling proteins in single cells. *Science* **287**, 1652–1655 (2000).
11. Elowitz, M. B., Levine, A. J., Siggia, E. D. & Swain, P. S. Stochastic gene expression in a single cell. *Nature* **297**, 1183–1187 (2002).
12. Rosenfeld, N., Young, J. W., Alon, U., Swain, P. & Elowitz, M. B. Gene regulation at the single-cell level. *Nature* **307**, 1962–1965 (2005).
13. Kalir, S. *et al.* Ordering genes in a flagella pathway by analysis of expression kinetics from living bacteria. *Science* **292**, 2080–2083 (2001).
14. Aldrige, P. & Hughes, K. T. Regulation of flagellar assembly. *Curr. Opin. Microbiol.* **5**, 160–165 (2002).
15. Swain, P. S., Elowitz, M. B. & Siggia, E. D. Intrinsic and extrinsic contributions to stochasticity in gene expression. *Proc. Natl Acad. Sci. USA* **99**, 12795–12800 (2002).
16. Swain, P. S. Efficient attenuation of stochasticity in gene expression through post-transcriptional control. *J. Mol. Biol.* **344**, 965–976 (2004).
17. Paulsson, J. Summing up the noise in gene networks. *Nature* **427**, 415–418 (2004).
18. Dekel, E. & Alon, U. Optimality and evolutionary tuning of the expression level of a protein. *Nature* **436**, 588–592 (2005).
19. Bray, D., Levin, M. D. & Morton-Firth, C. J. Receptor clustering as a cellular mechanism to control sensitivity. *Nature* **393**, 85–88 (1998).
20. Webre, D. J., Wolanin, P. M. & Stock, J. B. Bacterial chemotaxis. *Curr. Biol.* **13**, 47–49 (2003).
21. Raser, J. M. & O’Shea, E. K. Control of stochasticity in eukaryotic gene expression. *Science* **304**, 1811–1814 (2004).
22. Becskei, A. & Serrano, L. Engineering stability in gene networks by autoregulation. *Nature* **405**, 590–593 (2000).
23. Sourjik, V. & Berg, H. C. Receptor sensitivity in bacterial chemotaxis. *Proc. Natl Acad. Sci. USA* **99**, 123–127 (2002).
24. Sourjik, V. & Berg, H. C. Localization of components of the chemotaxis machinery of *Escherichia coli* using fluorescent protein fusions. *Mol. Microbiol.* **37**, 740–751 (2000).
25. Sourjik, V. & Berg, H. C. Functional interactions between receptors in bacterial chemotaxis. *Nature* **428**, 437–441 (2004).
26. Turner, L., Caplan, S. R. & Berg, H. C. Temperature-induced switching of the bacterial flagellar motor. *Biophys. J.* **71**, 2227–2233 (1996).
27. Blat, Y., Gillespie, G., Bren, A., Dahlquist, F. W. & Eisenbach, M. Regulation of phosphatase activity in bacterial chemotaxis. *J. Mol. Biol.* **284**, 1191–1199 (1998).
28. Almog, G., Stone, L. & Ben-Tal, N. B. Multi-stage regulation, a key to reliable adaptive biochemical pathways. *Biophys. J.* **81**, 3016–3028 (2001).
29. Scharf, B. E., Fahrner, K. A., Turner, L. & Berg, H. C. Control of direction of flagellar rotation in bacterial chemotaxis. *Proc. Natl Acad. Sci. USA* **95**, 201–206 (1998).
30. Raser, J. M. & O’Shea, E. K. Noise in gene expression: origins, consequences, and control. *Science* **309**, 2010–2013 (2005).

Supplementary Information is linked to the online version of the paper at www.nature.com/nature.

Acknowledgements We thank T. Shimizu, M. D. Levin, K. Lipkow and F. Geier for comments on the manuscript, and C. Bechinger, S. Bleil and S. Schulmeister for technical help. This work was supported by ZMBH funding, DFG grants to V.S. and K.B., and the BMBF project ‘Systems of Life–Systems Biology’.

Author Contributions V.S. designed the experiments and L.L. carried them out. M.K. performed the mathematical modelling together with K.B. The paper was written by M.K. and V.S. with comments from J.T. L.L. and K.B. contributed equally to this work.

Author Information Reprints and permissions information is available at npg.nature.com/reprintsandpermissions. The authors declare no competing financial interests. Correspondence and requests for materials should be addressed to M.K. (markus.kollmann@fdm.uni-freiburg.de) or V.S. (v.sourjik@zmbh.uni-heidelberg.de).